Design of a Lateral-Line Sensor for an Autonomous Underwater Vehicle

Nora Martiny, Stefan Sosnowski, Kolja Kühnlenz, Sandra Hirche *
Yimin Nie, Jan-Moritz P. Franosch, J. Leo van Hemmen **

* *Institute of Automatic Control Engineering, Munich, 80290 Germany*
(e-mail: sosnowski@tum.de).
** *Physik Department T35, Technische Universität München,*
85747 Garching bei München, Germany (e-mail: jfranosc@ph.tum.de).

Abstract: In an ongoing research project an autonomous underwater vehicle is to be built that will detect, localize, and avoid objects by means of a fully passive sensory system. Using hot-wire anemometry it measures local water velocities at the vehicle's hull and thus mimics the lateral-line system of fish and many amphibians. Fish often use the lateral-line system as their only means for navigation, especially under poor visual conditions. Simulations and theoretical calculations of the flow around an underwater vehicle show that velocity measurements with hot-wire anemometers enable an underwater vehicle to detect surfaces, so that no clear sight or active scanning is necessary for collision avoidance. A first series of experiments validates theoretical calculations and shows that a vehicle can detect parallel movement to a wall.

Keywords: artificial lateral line, autonomous underwater vehicle (AUV), object avoidance, Mexican cave fish *Anoptichthys jordani*, underwater sensors

1. INTRODUCTION

Just after hatching the blind Mexican cave fish (*Anoptichthys jordani*) has well-developed eyes, but does not react to visual stimuli. The eyes degenerate later. Nevertheless, the fish is able to avoid (navigate around) objects in its aquatic environment. It appears to "perceive" the objects as it passes by (Teyke, 1985; Abdel-Latif et al., 1990).

In the ongoing research project the authors analyze hydrodynamic stimuli as they arrive at *Anoptichthys jordani's* lateral-line system during object avoidance. Hydrodynamic stimuli have been calculated approximately. For a technical demonstration an underwater vehicle is built. The vehicle will use a sensory system based on the lateral-line system of fish and many other aquatic animals. The sensory system shall detect surfaces under water and also, if possible, smaller objects, by measuring the changes in local water velocity caused by these objects. The underwater vehicle shall then change direction accordingly so as to avoid collisions.

Fields of possible applications for such a vehicle could be turbid water with very poor vision as in canalization, pits filled up with water, and swamped buildings. Even under good visual conditions the lateral-line system is useful to avoid collisions and to relieve some burden from the camera system. Future applications of an underwater vehicle equipped with a lateral-line system could therefore be surveying and mapping of waters where humans cannot dive, e.g., because of poor vision, narrow space, or danger of collapse.

2. RELATED WORK

The lateral-line organ of fish and its functionality has been (and still is) investigated in a variety of fields, ranging from biology to neurology, biophysics and engineering. Previous work has covered the neurological aspects of information processing in lateral-line systems (Bleckmann, 1994; Coombs et al., 2000; Franosch et al., 2005; Goulet et al., 2007; Curcic-Blake and van Netten, 2006). At the University of Illinois at Urbana-Champaign scientists (Fan et al., 2002) are trying to build an artificial lateral-line sensor by replicating the hair cells using MEMS technology. A water flow parallel to the sensor bends the cilium in flow direction and a strain sensor surveys the deflection which in turn depends on water velocity. Another fish-like system, which is related in its functionality to the lateral-line organ, has been subject to research at the California Institute of Technology, Pasadena (MacIver et al., 2004). Finally, during evolution, the weakly electric black ghost knifefish (*Apteronotus albifrons*) has developed a system to sense its surroundings by a weak (approximately $1\,\mathrm{mV/cm}$) self-generated electric field causing voltage perturbations due to the difference in electrical conductivity between an object and water.

3. AUV CONCEPT

The development of an autonomous underwater vehicle (AUV) is an educational student project. Therefore, and due to the desire for a small-scale, highly maneuverable, modular AUV, most of the components are self-developed and self-built. Each subsystem is a separate module that communicates over CAN bus. In a later stage of the project the vehicle will consist of stackable modules containing
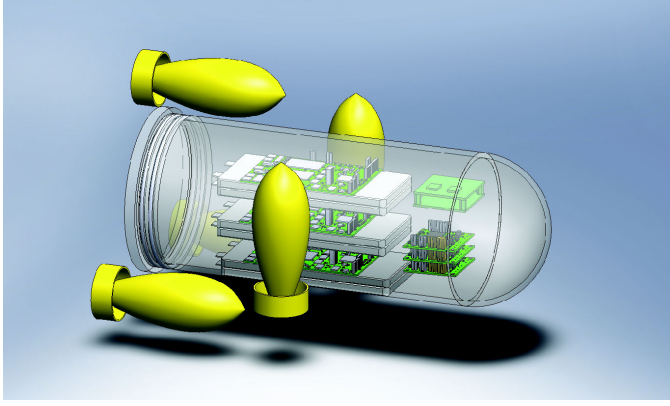
Fig. 1. AUV CAD: Conceptual 3D drawing of the vehicle.

the subsystems. Up to now an acrylic tube with diameter 14 cm and length 24 cm will house all modules. The AUV is composed of the following subsystems.

Propulsion The propulsion system consists of five encapsulated thrusters driven by brushed DC-motors. Each thruster can generate thrust up to 7 N. They are controlled by three motor-controller units that receive their commands via a CAN bus. Three of the motors are planned to face in the forward direction of the AUV, placed around the tube on the corners of an equilateral triangle. In this configuration forward and backward motion can be controlled, as well as pitch and yaw angles. The remaining two motors are placed perpendicular to the triangle configuration, controlling up- and downward movement and the roll angle. The placement of the motors enables control over 5 out of 6 possible degrees of freedom, making the robot highly maneuverable, whilst being able to compensate external disturbances directly (besides lateral disturbances).

Energy management The robot is powered by 12×3.7 V lithium polymer accumulators with 10 Ah each, resulting in a total of 20 Ah at 22.2 V nominal voltage. Lithium polymer accumulators were chosen for their high energy density and their capability of producing a high current. Due to the risks involved with lithium polymer technology and for providing status information, the authors have developed an energy management system that takes care of monitoring the cells and ensuring safety during charging or discharging. Voltage and current status are available via a CAN bus and LCD display.

Pressure sensor array To determine the absolute diving depth a pressure sensor array is used, with four sensors distributed on the robot.

Processing unit and inertia measurement unit The main processing unit is a 60 MHz ARM7 processor coupled with an inertia measurement unit from Ascending Technologies. In the inertia measurement unit sensor data from three MEMS gyroscopes, a three-axis acceleration sensor, a three-axis magnetometer and the pressure data is fused and passed on in preprocessed form to the command unit for stable and reliable angular and translational data. For position tracking at the surface a GPS module is included, as well as a wireless Zigbee transceiver for communication with the operator.
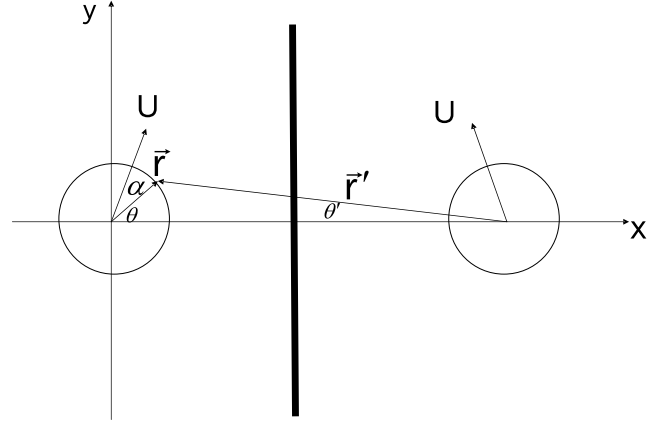

Fig. 2. A mirrored sphere to satisfy the boundary condition at the wall.

Lateral-line sensor system The proposed lateral-line sensor system, installed on the frontal hemisphere, will detect objects in such a way that the vehicle can avoid collisions. The installation on the front part provides laminar flow and maximum distance to the turbulence inducing thrusters. It is planned to install an array of up to 40 sensors.

4. THEORETICAL CALCULATION OF THE FLOW AROUND THE VEHICLE

We approximate the underwater vehicle by a sphere with radius a whose center has a distance D from a wall. The boundary condition that water flows only parallel to the wall is satisfied by introducing a "mirror" sphere that moves in the mirrored direction at the opposite side of the wall, see Fig. 2.

This approach is an approximation insofar as the boundary condition at the surface of the first sphere is disturbed by the presence of the second sphere and thus boundary conditions are only satisfied approximately. The approximation is exact for the limit case $a \to 0$ or $D \to \infty$.

A moving sphere with radius a and velocity $\boldsymbol{U}$ that currently passes the origin of the coordinate system in an incompressible ideal fluid causes a velocity field $\boldsymbol{v}(\boldsymbol{r})$ that can be described by a velocity potential (Lamb, 1932)

$$\varphi_0(\boldsymbol{r}) = \frac{a^3}{2|\boldsymbol{r}|^3} \boldsymbol{U} \cdot \boldsymbol{r}$$

such that

$$\boldsymbol{v}(\boldsymbol{r}) = -\operatorname{grad} \varphi_0(\boldsymbol{r}) .$$

Say the left sphere in Fig. 2 is causing a velocity potential φ_0 and the "mirror" sphere is causing a velocity potential φ'. Then the total velocity potential is

$$\varphi = \varphi_0 + \varphi' = \frac{a^3}{2r^3} \boldsymbol{U} \cdot \boldsymbol{r} + \frac{a^3}{2r'^3} \boldsymbol{U}' \cdot \boldsymbol{r}' .$$

In case the sphere is moving parallel to the wall the condition $\boldsymbol{U} \cdot \boldsymbol{r} = \boldsymbol{U}' \cdot \boldsymbol{r}'$ holds, therefore

$$\varphi = \frac{a^3(\boldsymbol{U} \cdot \boldsymbol{r})}{2r^3} \left[1 + (\frac{r}{r'})^3 \right] .$$

Using a polar coordinate system (r, θ), cf. Fig. 2, one gets

$$\varphi = \frac{a^3 U \sin \theta}{2r^2} \left[1 + \frac{r^3}{(r^2 + 4D^2 - 4Dr \cos \theta)^{3/2}} \right]$$

where D is the distance of the center of the sphere to the wall. The velocity v_θ in θ-direction then is

$$v_\theta = \frac{1}{r}\frac{\partial \varphi}{\partial \theta} =$$
$$= \frac{a^3 U \cos\theta}{2r^3} + \frac{a^3 U}{2}\frac{(r^2 + 4D^2)\cos\theta - 2Dr\sin^2\theta - 4Dr}{(r^2 + 4D^2 - 4Dr\cos\theta)^{5/2}}$$

As water flow lies within the plane of projection in Fig. 2, for $r = a$ and $\theta \in \{0, \pi\}$, one gets the water velocities parallel to the surface of the sphere

$$|v_0| = \frac{U}{2}\left[1 + \frac{a^3}{(2D-a)^3}\right],$$
$$|v_\pi| = \frac{U}{2}\left[1 + \frac{a^3}{(2D+a)^3}\right]$$

at the point closest to the wall ($\theta = 0$) and the opposite point ($\theta = \pi$). Using the abbreviation $\delta := D/a$, we can also write

$$|v_0| = \frac{U}{2}\left[1 + \frac{1}{(2\delta-1)^3}\right]$$
$$|v_\pi| = \frac{U}{2}\left[1 + \frac{1}{(2\delta+1)^3}\right].$$

The velocity difference $\Delta v = |v_0| - |v_\pi|$ between the point on the sphere nearest to the wall and opposite to the wall is then

$$\Delta v = \frac{U}{2}\left[\frac{1}{(2\delta-1)^3} - \frac{1}{(2\delta+1)^3}\right].$$

In an undisturbed system, i.e. without wall or a wall at infinite distance, $|v_0| = |v_\pi| = U/2$ and $\Delta v = 0$. For $\delta = 1$, i.e. distance of the hull to the wall is zero, $\Delta v = 48\,\% \, U$. For $\delta = 2$, $\Delta v = 1.5\,\% \, U$. So far, we have calculated all velocities in the coordinate system of the laboratory. The sensors on the vehicle, however, measure the water velocity *relative* to the vehicle. In the coordinate system of the sphere

$$|v_0^{\mathrm{sphere}}| = \frac{U}{2}\left[3 + \frac{1}{(2\delta-1)^3}\right]$$
$$|v_\pi^{\mathrm{sphere}}| = \frac{U}{2}\left[3 + \frac{1}{(2\delta+1)^3}\right] \quad (1)$$

and $\Delta v^{\mathrm{sphere}} = \Delta v$. To compare with experiments, we introduce the relative velocity difference

$$\Delta := \frac{|v_0^{\mathrm{sphere}}| - |v_\pi^{\mathrm{sphere}}|}{|v_0^{\mathrm{sphere}}| + |v_\pi^{\mathrm{sphere}}|}. \quad (2)$$

The relative velocity difference is only dependent on the ratio δ of the distance to the wall D and the radius a of the sphere, specifically

$$\Delta = \frac{\frac{1}{(2\delta-1)^3} - \frac{1}{(2\delta+1)^3}}{6 + \frac{1}{(2\delta-1)^3} + \frac{1}{(2\delta+1)^3}}. \quad (3)$$

As in an ideal fluid the velocity field constitutes instantaneously, all calculations above are also valid for a time-dependent velocity $U(t)$ of the sphere.
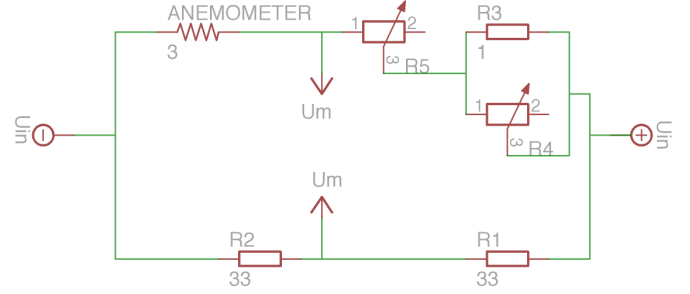

Fig. 3. Wheatstone bridge with two potentiometers for adjustment.

5. EXPERIMENTAL VALIDATION

5.1 Hot-wire anemometry

To measure fluid velocity one can exploit heat dissipation of a hot wire in the fluid. Heat dissipation P of a wire (or thermistor or sphere) of over-temperature ϑ in a fluid depends on the velocity v of the fluid,

$$P \approx (A + Bv^n)\vartheta \quad (4)$$

where $n \approx 0.5$ and the constants A and B depend on the geometry and the fluid (Bruun, 1996; Itsweire and Helland, 1983; Strickert, 1974). For a wire, there exist approximations for the constants A, B and n, e.g. (Strickert, 1974)

$$P \approx \left[0.42\left(\frac{\nu c_p \rho}{k}\right)^{0.2} + 0.57\left(\frac{\nu c_p \rho}{k}\right)^{0.33}\left(\frac{vd}{\nu}\right)^{0.5}\right]\pi l k\vartheta$$

where ρ is the density, c_p the specific heat capacity, k the heat conductivity, ν the kinematic viscosity of the fluid, d the diameter, and l the length of the wire.

In an aquarium with an apparatus that tracts a hot-wire through the water at different velocities, heat dissipation measured by the authors was in good agreement with (4) with $n \approx 0.2 \ldots 0.3$.

5.2 Hardware setup

Wheatstone Bridge The basic measuring system for thermal water flow sensors used here is the Wheatstone bridge, as shown in Fig. 3. Resistor R_1 and R_2 constitute the reference branch, with $R_1 = R_2 = 33\,\Omega$. A parallel connection of the potentiometer $R_4 = 10\,\Omega$ and the resistor $R_3 = 1\,\Omega$, in series with the potentiometer R_5 (with a maximum resistance of $R_5 = 10\,\Omega$), is for fine-tuning the Wheatstone bridge. *ANEMOMETER* stands for the heating element, which was a hot wire from FMP Technology. The wire consists of platinum and has a a diameter of $30\,\mu$m. The resistance of both wires used in experiments was $3.8\,\Omega$. Before performing each measurement, the voltage U_m across the bridge was tuned to $0\,$V ($\pm 2\,$mV).

AUV mockup A wooden sphere with a radius of $a = 7.5\,$cm is used as a model for an underwater vehicle, cf. Fig. 4.

The authors chose the spherical shape for simplicity and to be able to compare theoretical calculations with experiments. Two hot-wire sensors are fixed on two opposite
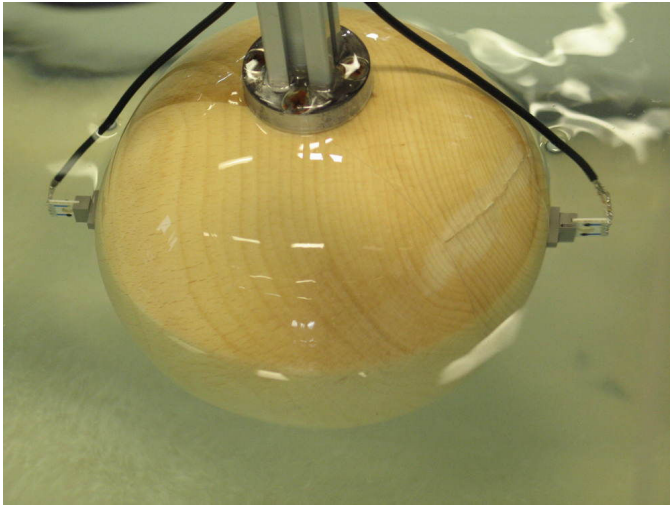
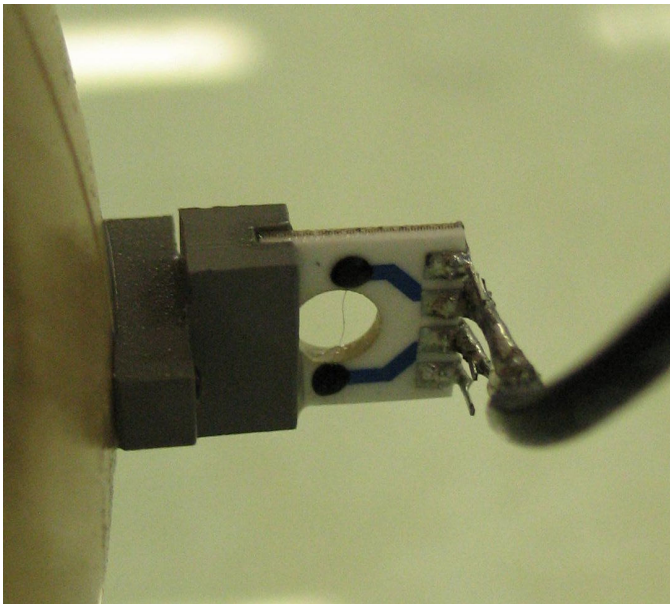Fig. 4. Wooden sphere used for experiments. The sensors are mounted on opposite sides of the sphere.

Fig. 5. Hot-wire sensor mounted on the sphere. The $30\,\mu$m thin wire is mounted in the round hole of a plastic casing.

sides of the sphere, normal to the water flow direction, cf. Fig. 5.

Each of the sensors is connected to a Wheatstone bridge as described above. The bridges are compensated at an input current of $I_{\text{in}} = 0.400\,$A resulting in an over-temperature of about $\vartheta = 130\,$K. Although the temperature of the wire is then much higher than the evaporating temperature of water no specific physical effects occurred and this over-temperature provided good results in former experiments.

To move the sphere, it is attached to a linear axis (Copley Controls Corp). Figure 6 shows the experimental setup. The linear axis is 1.8 m long and powered by a servo controller (Xenus), which regulates the force on the motor cart. The cart position is determined with an incremental encoder, feeding the impulses from the hall sensors on the linear motor to an analog to digital converter card (Sen-
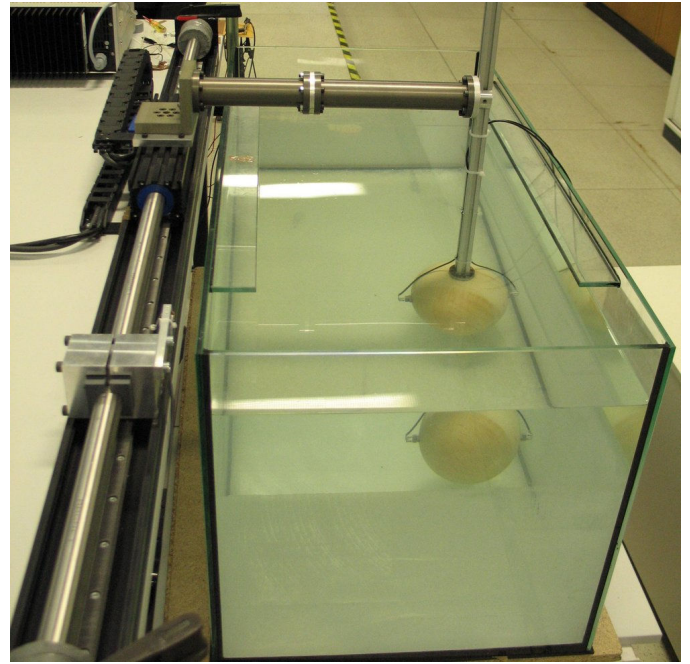

Fig. 6. Experimental setup. The motor on the linear axis (left) moves the sphere parallel to the walls of the aquarium.

soray). With this encoder the position can be measured in steps of $12.5\,\mu$m step size. In this experimental setup the axis is position-controlled by a high-gain proportional-derivate controller implemented in Matlab/Simulink. The input is the error of the measured position compared to the set position, the output the force command to the Xenus controller. Thus the sphere can be moved on precise trajectories by applying various signals on the controller set-point. In each experiment, the authors recorded voltage data for one minute without moving the sphere. The part of the data recorded during this period was later used to correct for constant voltage offset. After one minute, the sphere moved harmonically for five minutes with frequency $1\,$rad/s $= 1/(2\pi)\,$Hz and amplitude 5 cm, resulting in a velocity amplitude of 5 cm/s. The same procedure was used for the calibration measurements described below.

5.3 Data processing and calibration

The voltage across each Wheatstone bridge was digitized by a analog to digital converter card (Meilhaus ME-4670I) with 1000 samples per second. Measurement noise was about 1 mV and the authors got typical signals of about 50 mV. Measurement noise did not change visibly when short-circuiting the signal cable, thus most noise did come from from the converter card, not from the measurement apparatus. The linear motor, however, caused noise in the digitalized voltage signal, which appeared as single voltage spikes up to about 20 mV about every 100 ms. Therefore, the voltage signal was filtered with a first-order low-pass filter with a time constant of 50 ms. The first part of the voltage signal was always measured without moving the sphere. Although the Wheatstone bridges were adjusted to zero as well as possible, the part of the signal without movement was used to correct for mis-adjustment of the bridge by subtracting the mean of the part of the signal

without movement from the signal. All experiments were performed with constant current $I_{in} = 0.400\,\text{A}$ through the bridge, and thus the wire, and a bridge voltage of $U_{in} = 3.00\,\text{V}$ for each sensor. Since the resistors R_1 and R_2 are much larger than the resistance of the hot wire and the hot wire changes resistance only slightly, the current through the hot wire could be taken to be constant under all experimental conditions. At relatively slow velocities used here, we can neglect the dependence of the over-temperature on water velocity and thus voltage. The bridge was calibrated such that the bridge voltage was zero for water velocity zero. Thus, using equation (4), the bridge voltage U_m is dependent on water velocity v according to

$$U_m \sim v^n .$$

To determine the exponent n by a linear regression, one can take the logarithm on both sides of (5.3), which gives the relation

$$\ln v = \frac{1}{n} \ln U_m + C .$$

Velocity and bridge voltage data was collected by performing a sinusoidal motion of the sensor mounted on a thin rod (without sphere and in the middle of the aquarium). Velocity data was calculated from the position data of the linear axis by first filtering the position data with a linear filter as described above and a numeric differentiation afterwards. A linear regression was performed on that data resulting in $n = 0.29$.

As only *relative* velocities between sensors are needed to calculate Δ from (2), the authors have just taken

$$u := U_m^{1/n} \tag{5}$$

as a measure for relative velocities in arbitrary units. With u_1 being the velocity signal from the left sensor and u_2 from the right sensor the authors then calculated Δ by a linear regression using

$$u_1 - u_2 = \Delta(u_1 + u_2) \tag{6}$$

where u_1 and u_2 correspond to $|v_0|$ and $|v_\pi|$ of (2) (the hot wire can only measure absolute velocities). Figure 7 shows the voltages acquired during calibration and the corresponding filtered voltages. Figure 8 shows the corresponding velocity data acquired from the position sensor during calibration and, for comparison, calculated from voltage data.

5.4 Results of wall-detection experiments

To verify whether the theoretical model for wall-detection described above is implementable in a robot, several experiments have been performed with different distances of the sphere to the walls of the aquarium. The dimensions of the aquarium are $L \times W \times H = 100\,\text{cm} \times 50\,\text{cm} \times 50\,\text{cm}$. For each experiment, the voltage U_m across the bridge was captured and the corresponding water velocity has been calculated using the methods described above. Figure 9 shows typical velocity data.

Figure 10 shows the relative velocity difference Δ from (2) in dependence on the relative distance δ to the wall. The velocity difference increases as the distance to the wall decreases and the water velocity at the sensor next to the wall is higher, in accordance with theory. The effect has also about the same magnitude as theory predicts, but sets
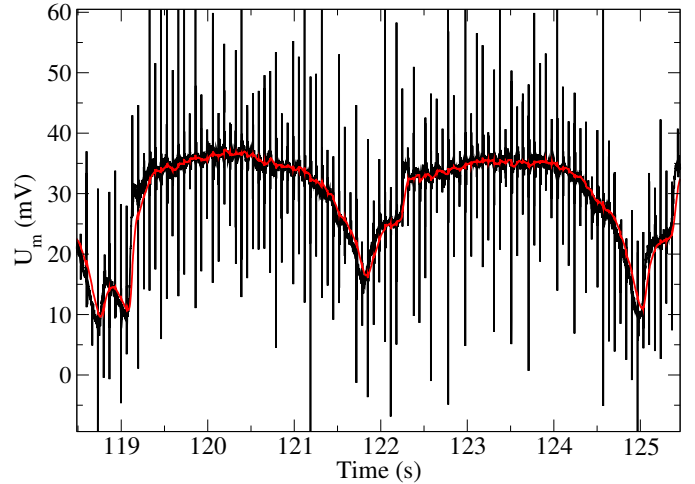

Fig. 7. Voltage U_m (black) across the bridge acquired during sensor calibration. As the motor of the linear axis used to move the sensor caused a lot of noise that appeared as separated voltage spikes, all voltage data was filtered by a first order low-pass filter (red) before calculating the corresponding water velocities.
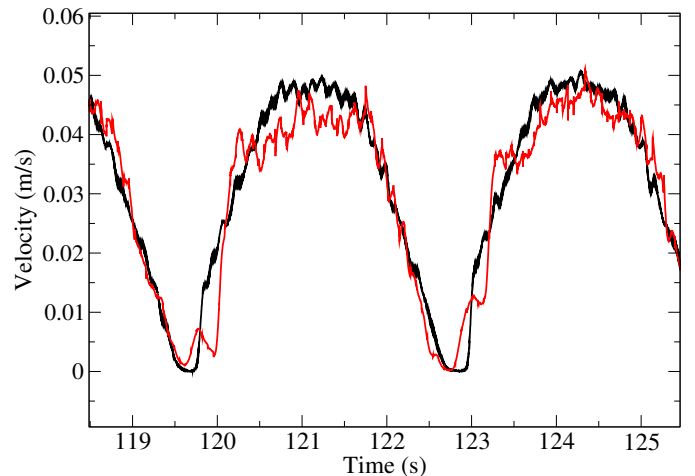

Fig. 8. Velocity (black) of the sensor during calibration calculated from the position sensor of the axis. It fits rather well with the velocity (red) calculated by the corresponding voltage from Fig. 7.

in a bit earlier, i.e. already at larger distances from the wall in contrast to theory. This may be due to the fact that the sensor was mounted about 1 cm away from the surface of the sphere. However, further experiments and calculations have to be performed to decide whether the discrepancies to theory are due to measurement errors or real physical effects.

6. CONCLUSION AND FUTURE WORK

The authors propose an artificial lateral-line sensor system for an autonomous underwater vehicle based on hot-wire anemometry. Measurements have proven that this concept is technically feasible and that the sensitivity required can be calculated by the present theory although the theory neglects viscosity causing boundary layer effects and turbulence. Sensitivity strongly depends on signal-to-noise ratio. Measurement noise in the current setup is
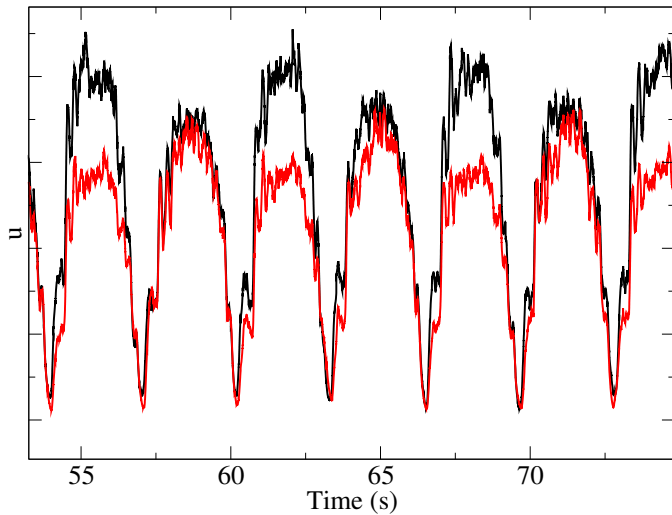
Fig. 9. Velocity data u in arbitrary units calculated using (5) for a measurement where the sphere was moving at a distance $D = 10.1\,\text{cm}$ ($\delta = D/a = 1.35$) from the left wall. Water velocity at the left sensor (black) is higher than at the right sensor (red) in accordance with the theory in (1). The data shows a relatively large velocity difference between forward and backward motion. This was observed in every measurement with the sphere but not during calibration. The effect may be due to slight asymmetries in the measurement apparatus, e.g. that the sphere was not exactly aligned to the direction of motion or the anemometer wires not exactly aligned parallel to the surface of the sphere and perpendicular to the direction of motion.
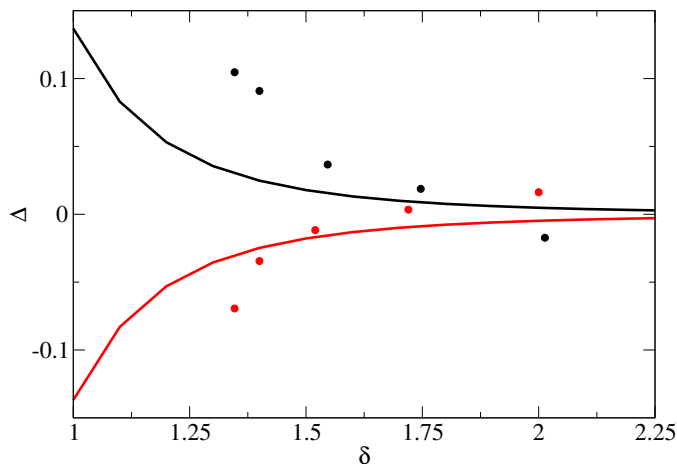

Fig. 10. Relative velocity differences Δ from measurements (dots) compared to the theory in equation (3) (solid lines). If the velocity difference between left and right sensor was negative, Δ got a negative sign (red data) and a positive sign otherwise (black data). Thus the experiments resulting in the red dots were made with the sphere moving closer to the left wall and the black dots were measured with the sphere moving closer to the right wall. Qualitatively, the data matches with the theoretical calculations.

dominated by the analog to digital converter card which causes noise with a root mean square of about $1\,\text{mV}$. In addition, the motor of the linear axis is responsible for much of the noise that occurs during motion of the sphere. In future experiments, signal to noise ratio has to be further improved to be able to measure fluid flow under the natural condition when the vehicle is approaching a wall.

REFERENCES

Abdel-Latif, H., Hassan, E. S., von Campenhausen, C., 1990. Sensory performance of blind mexican cave fish after destruction of the canal neuromasts. Naturwiss. 77, 237–239.

Bleckmann, H., 1994. Reception of Hydrodynamic Stimuli in Aquatic and Semiaquatic Animals. Fischer, Stuttgart.

Bruun, H. H., 1996. Hot wire anemometry. Oxford Univ. Press, Oxford.

Coombs, S., Finneran, J. J., Conley, R. A., 2000. Hydrodynamic image formation by the peripheral lateral line system of the Lake Michigan mottled sculpin, *Cottus bairdi*. Phil. Trans. R. Soc. Lond. B 355 (1401), 1111–1114.

Curcic-Blake, B., van Netten, S. M., 2006. Source location encoding in the fish lateral line canal. J. Exp. Biol. 209, 1548–1559.

Fan, Z., Chen, J., Zou, J., Li, J., Liu, C., Delcomyn, F., 2002. Development of artificial lateral-line flow sensors. Solid-State Sensor, Actuator and Microsystem Workshop 0-9640024-4-2, 169–172.

Franosch, J.-M. P., Sichert, A. B., Suttner, M. D., van Hemmen, J. L., 2005. Estimating position and velocity of a submerged moving object by the clawed frog *Xenopus* and by fish — a cybernetic approach. Biol. Cybern. 93 (4), 231–238.

Goulet, J., Engelmann, J., Chagnaud, B. P., Franosch, J.-M. P., Suttner, M. D., van Hemmen, J. L., 2007. Object localization through the lateral-line system of fish: Theory and experiment. J. Comp. Physiol. A 194 (1), 1–17.

Itsweire, I. C., Helland, K. N., 1983. A high-performance low-cost constant-temperature hot-wire anemometer. J. Phys. E-Scien. Inst. 16 (6), 549–553.

Lamb, H., 1932. Hydrodynamics, 6th Edition. Cambridge University Press, Cambridge.

MacIver, M. A., Fontaine, E., Burdick, J. W., 2004. Designing future underwater vehicles: Principles and mechanisms of the weakly electric fish. IEEE Journal of Oceanic Engineering 29 (3), 651 – 659.

Strickert, H., 1974. Hitzdraht- und Hitzfilmanemometrie. VEB Verlag Technik, Berlin.

Teyke, T., 1985. Collision with and avoidance of obstacles by blind cave fish anoptichthys jordani (characidae). J. Comp. Physiol. A 157, 837–843.